Three-Dimensional Profiling of OLED by Laser Desorption Ionization-Mass Spectrometry Imaging

Andrew E. Paulson, Trevor T. Forsman, Young Jin Lee*

Department of Chemistry, Iowa State University, Ames, IA 50011, USA

ABSTRACT: Organic light emitting devices (OLEDs), especially in a screen display format, present unique and interesting substrates for Laser Desorption/Ionization - Mass Spectrometry Imaging (LDI-MSI) analysis. These devices contain many compounds that inherently absorb light energy and do not require an additional matrix to induce desorption and ionization. OLED screens have lateral features with dimensions that are tens of microns in magnitude and depth features that are tens to hundreds of nanometers thick. Monitoring the chemical composition of these features is essential, as contamination and degradation can impact device lifetime. This work demonstrates the capability of LDI-MSI to obtain lateral and partial depth resolved information of multicolored OLED displays and suggests the application to other mixed organic electronics with minimal sample preparation. This was realized when analyzing two different manufactured OLEDs, in an active-matrix display format, without the need to remove the cathode. By utilizing low laser energy and high lateral spatial resolution imaging (10 µm), depth profiling can be observed while maintaining laterally resolved information resulting in a three-dimensional MSI approach that would complement existing OLED characterization methods.

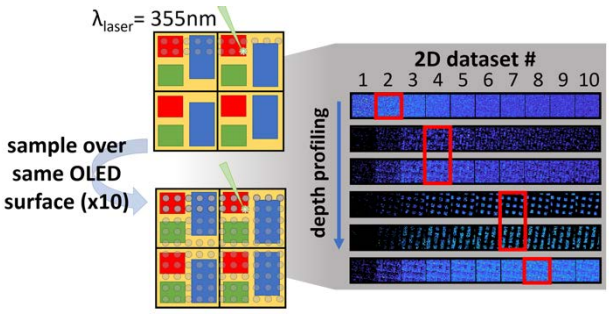

KEYWORDS: *Laser Desorption/Ionization, Mass Spectrometry Imaging, Depth profiling, Organic Light Emitting Device*

INTRODUCTION

Organic light emitting devices (OLEDs) are prominent in consumer, research, and industrial applications ranging from energy efficient light bulbs to high definition screens for computers. The devices have come a long way since the advent of the first thin low voltage multilayer OLED produced by Tang and VanSlyke of Kodak in the 1980s.[1,2] Many other advancements allowed for OLEDs to become so pervasive, including but not limited to: the development of white light OLEDs,[3] incorporation of dopants in the emitting layer[4,5], demonstration of nearly 100% internal quantum efficiency for phosphorescent emitting materials[5,6], and the development of robust dynamic drive devices.[7] Collectively, the work has allowed for the commercialization of efficient and durable OLED displays.

OLED display fabrication involves discontinuous layering of organic, organometallic, and inorganic materials. These materials have tuned highest occupied molecular orbital (HOMO), lowest occupied molecular orbital (LUMO), and Fermi levels to allow for unhindered electron and hole transfer through the device, permitting exciton generation within the light emitting layer in the center of the layered stack.[8] These layers are deposited in thicknesses ranging from a few nanometers to a couple hundred nanometers, resulting in devices with functional components that are of sub-micron thickness in total. Generally, OLED displays found in common commercial applications are comprised of pixels corresponding to white, red, green, or blue emitted light. The lateral dimensions of these pixels determine the image resolution of the screen and are typically tens of micrometers in magnitude. The integrity of the OLED architecture is critical for successful and prolonged operation.

The OLED lifetime is dependent on degradation pathways that are extrinsic (failed encapsulation, contaminants, fabrication environment, substrate abnormalities, and operating conditions) and intrinsic (electrochemical, thermal, interfacial, photochemical, carrier/charge balance, exciton density, migration, and dipole reorientation).[9,10] Extrinsic degradation can lead to dark spots or complete failure of the screen due to shorting within the OLED structure; however, near perfect fabrication and encapsulation processes have largely removed these issues.[11,12] Extrinsic degradation processes can also be mitigated by shortening the fabrication process.[13] Penconi *et al.* have demonstrated complimentary liquid chromatography-mass spectrometry, differential scanning calorimetry, and photo luminescent protocols to evaluate degradation pathways of iridium complexes, commonly used in the emitting light layer due to color tunability, during device operation.[14,15] There is also interest in degradation processes that occur between compounds in layers proximate to one another, such as the complexation between the emitting compounds and the hole blocking layer.[14,16,17] These are a few examples of the interest in intrinsic degradation. Consequently, methods that provide both spatial and depth resolved chemical information assist the analyst in assessing the quality of the OLED through locating degradation and contamination within the OLED structure and making appropriate interventions to improve the device.

Ideally, an analytical technique would give chemical information with lateral and depth resolved information with minimal impact on the analytes. Many analytical methods have been deployed to assess depth features of OLEDs including dynamic x-ray photoelectron spectroscopy[18–20], secondary ion mass spectrometry (SIMS)[19,21–23], and laser desorption/ionization-mass spectrometry (LDI-MS).[17,24] The two most common mass spectrometry based analytical approaches for lateral and depth information include time-of-flight SIMS (TOF-SIMS) and LDI-MS. The differences in spectral information obtained from these techniques are largely determined by the limitations of the respective ionization source. Though SIMS provides better resolution of depth information, higher energy associated with ion beams leads to more significant fragmentation of analytes which can abet ambiguous assignments when dealing with OLED layers that have compounds with identical or similar fragments. SIMS also has high vacuum requirement where some LDI-MS uses milder vacuum conditions allowing for the analysis of degradation and contamination analytes that have higher volatility.

LDI-MS can be used as a label free imaging technique that can map lateral analyte distributions within a sample. Mass spectrometry images are acquired by rastering a laser over a sample surface and analyzing analytes desorbed/ionized with a mass analyzer. Each sampling results in a mass spectrum and knowing the lateral position of the sampling allows the analyst to generate heat maps of ion intensity for *m/z* values of interest. The technique has been used in biological systems to image distributions of analytes, with relatively high auto-ionization efficiency, in various tissue types across a variety of analytes including metabolites and nanomaterials.[25-27] So long as the analyte of interest meets the caveat of auto-ionization when irradiated with the laser, the LDI-MS method can be utilized.

It has been shown that LDI-MS can be applied to depth profiling analysis of mixed organic electronics, including photovoltaic panels and OLEDs, without special sample preparations in order to determine composition, contaminants, and degradation products arising from operation.[24,28] Scholz *et al.* have demonstrated that LDI-MS can be used to assess the projected lifetime of an OLED by obtaining the intensity ratio of an emitter degradation ion, formed by complexation with a compound from a neighboring layer, compared to the emitter-fragment ion.[17] LDI-MSI of a single color OLED has also been applied to imaging degradation products after device exposure to air.[29] The use of laser to deplete thin surface layers has been previously demonstrated to obtain MS images of deeper layer in plant tissues.[30] However, to the best of our knowledge, the use of LDI-MSI as a means of simultaneously obtaining lateral and depth profiling information, especially on commercial OLED screens, has not been reported. Furthermore, OLEDs are a particularly unique candidate for lateral and depth profiling by laser desorption due to their relative structural and chemical simplicity when compared to more complex systems like biological samples. Herein, we demonstrate the ability to use LDI-MSI to obtain both lateral and partial depth information regarding the composition of OLED display screens.

EXPERIMENTAL SECTION

MALDI-MSI

Two OLED screens, OLED A and OLED B, were obtained from Samsung Display, Asan, South Korea. OLED A is manufactured for lower resolution type applications and is used in automobile displays. OLED B is manufactured for higher resolution applications and is used in cellular phone displays. The OLED screens were cut to fit an LDI slide sample holder and the top protective polarized glass layer was removed prior to analysis. No further sample preparation was required, and analysis was performed promptly after removing the protective glass. Optical images of the OLED surfaces were obtained with an OLYMPUS BX53 microscope using a home-built reflection microscope setup. Optical images were obtained using a 20x objective lens and measurements were made with cellSens software (**Figure S1**).

MS analysis was performed on a MALDI-linear ion trap-Orbitrap (Thermo Scientific, San Jose, CA) in positive mode. Details of this instrument can be found in the original paper by Strupat et. al.[31] Briefly, the source pressure is maintained at 75 mTorr during MALDI operation filled with nitrogen gas (99.999%). The sample stage movement has an accuracy of approximately 1µm according to Strupat *et al*. We replaced the original N_2 laser with an external diode-pumped Nd:YAG laser (Elforlight, Daventry, England)) as described elsewhere.[32]

For the data shown in this work, no matrix was applied. A 355 nm Nd:YAG laser (Elforlight, Daventry, England) was rastered across the OLED surface, using a 10 µm raster step over a 410 µm x 410 µm area for OLED A and 400 µm x 400 µm area for OLED B. The laser spot size was 10 µm. The same area was passed over ten consecutive times to generate ten two-dimensional (2D) datasets. Each 2D dataset took approximately 27 minutes to acquire, resulting in a total analysis time of 4.5 hours. Three different laser power settings and three different laser shot per scan settings were tested for depth profiling laser optimization. A summary of the optimization experiments for OLED A are in the supplementary information (**Figure S2 and S3).** The lowest intensity setting that resulted in reproducible signal provided the best resolution of depth features. Thus, a laser intensity 88% (0.82 ±0.07 µJ/pulse at sample surface) with 10 laser shots per scan and an 88% laser intensity with 5 laser shots per scan provided the optimal imaging and depth profiling conditions for OLED A and OLED B, respectively. The laser shot frequency for both samples was set to 60 Hz with a pulse duration of 4 ns. Data was processed with ImageQuest and Xcalibur (Thermo Scientific, San Jose, CA). Two dimensional and three-dimensional MS images were generated with MSiReader (v1.01 and v1.02b, respectively).[33]

Desorption electrospray ionization (DESI)-MS

Depth profiling of OLED A was performed using DESI-MS in the positive ion mode to compare with the results obtained with LDI-MS. A DESI 2D system (Prosolia, Indianapolis, IN) was used in conjunction with a quadrupole-Orbitrap hybrid mass spectrometer (Q Exactive Orbitrap; Thermo Scientific, San Jose, CA). The DESI solvent used to gently dissolve the OLED device was a mixture of acetonitrile, water, chloroform, and tetrahydrofuran (70:20:5:5 in volume). The DESI parameters are as follows: ESI voltage of 3 kV, the spray impact angle of 57º, MS inlet temperature of 300 ºC, solvent flow rate of 2.0 µL/min, and raster step size of 100 µm. The distances between DESI tip, sample surface, and MS inlet were optimized to achieve the best signal. Data was processed with Xcalibur (Thermo Scientific, San Jose, CA).

RESULTS AND DISCUSSION

OLED sample structure

The layers and pixel configurations for the two OLEDs investigated are summarized in the schematics shown in **Figure 1**. Full explanation of layer function and fabrication is not described as it is outside the scope of this work, though a more complete description of OLEDs in general can be found elsewhere.[8] The cathode, anode, and electron injection layer (EIL) consist of inorganic material and are not readily observed with the LDI-MS method. The capping layer (CPL) and all remaining layers have proprietary organic and organometallic compounds that have the potential for being observed during LDI-MS analysis. Pixel specific compounds are exclusively found in the emission material layer (EML) and should have lateral distributions that match the manufactured pixel geometries. The EML consists of the blue dopant, green dopant, and red dopant, which are responsible for generating the light after excitation in the respective host compounds: blue host, green host, and red host. Herein, EML compounds will be referred to with the convention xEML#, where "x" is the pixel color blue (B), green (G), or red (R), and the "#" being a number assignment to index one of the compounds in a pixel. The number designation is also used to index compounds in the ETL in OLED A. Note that the explicit designation of host or dopant is being avoided, unless necessary, in order to protect proprietary information. All other layers, the CPL, electron transport layer (ETL), hole transport layer (HTL), and hole injection layer (HIL), are evenly layered across the device during fabrication. In this study, we raster the laser across the same OLED surface multiple times to obtain 2D datasets at various depth. As the materials are depleted for each 2D data acquisition, this approach will allow for the resolution of some depth information of the OLED screen while maintaining lateral distribution information for pixel compounds. The laser spot size (10 µm) and raster step size (10 µm) are closely matched, so that there is no overlap. The laser spot position is quite reproducible for subsequent scanning of small area (0.4x0.4 mm^2) as the stage motor accuracy is about 1 µm.[31] However, due to thermal diffusion caused by laser induced heating, there is some inevitable mixing of deeper layers within the OLED architecture. This diffusion limits the ability to completely resolve depth features.

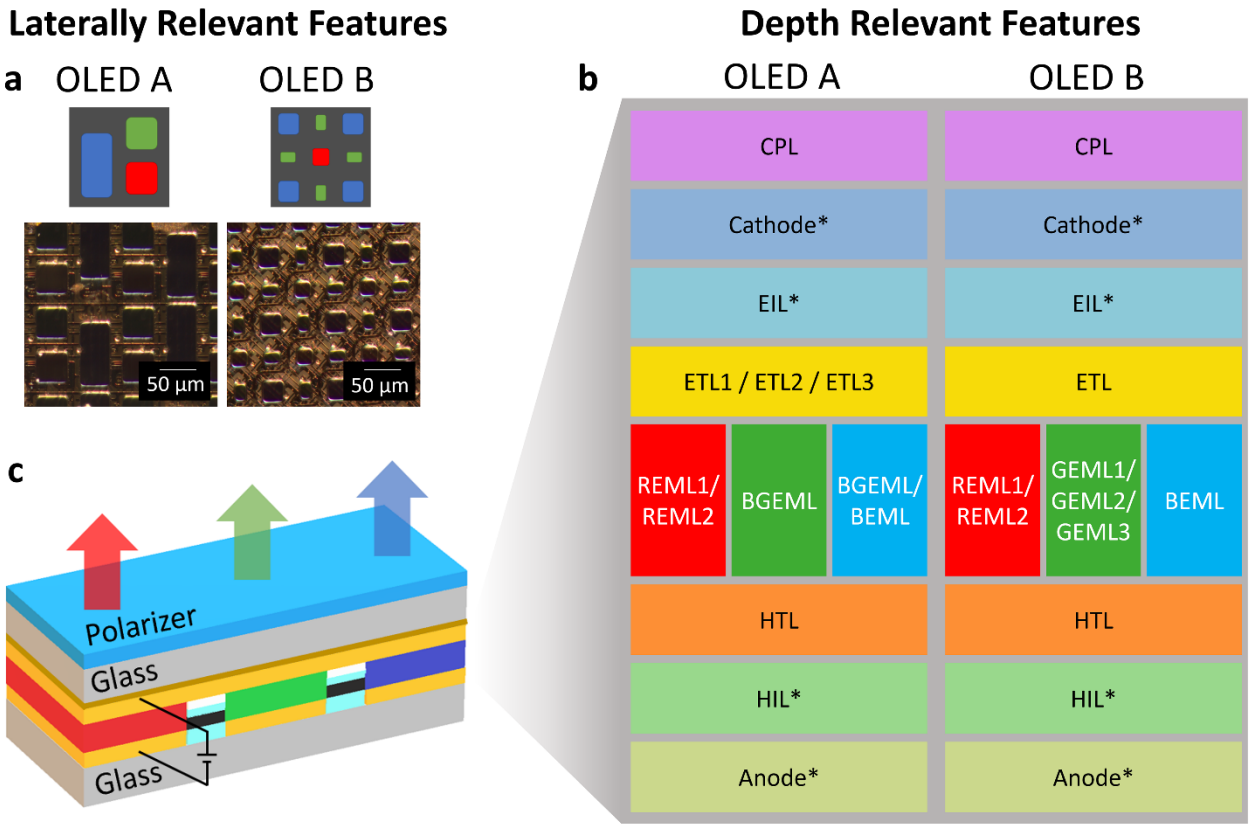

Figure 1. (a) Schematic and optical image of laterally relevant features, the pixel geometries, for the OLEDs investigated. **(b)** Schematic of depth relevant features, the layered architecture, of the OLEDs investigated. **(c)** Cross section schematic of a fabricated OLED screen during operation. The following abbreviations were used: CPL- capping layer, EIL- electron injection layer, ETL- electron transfer layer, BEML- blue emission material layer, GEML- green emission material layer, BGEML- blue/green emission material layer, REML- red emission material layer, HTL- hole transfer layer, and HIL- hole injection layer. Backslashes indicate that multiple compounds are present within the specified layer and asterisks indicate components that were not observed with the current method.

LDI-MSI Depth Profiling on OLED

The OLEDs were rastered across ten consecutive times to produce ten 2D datasets. The total sampled depth is estimated to be around 400nm from the top of the CPL to the bottom of the HTL. **Figure 2a** and **2b** show 2D MS images of a major component for each layer for OLED A and B, respectively. The *m/z* values and expected lateral localizations for compounds in OLED A and OLED B can be found in **Table S1** and **Table S2**,

respectively. Representative mass spectra from the 5th 2D dataset for each OLED can be seen in **Figure S4**. The analytes were monitored as molecular ions except for ETL1 and ETL2 in OLED A and the ETL in OLED B which are lithiated adducts. Not all layers in **Figure 1** have observable compounds using LDI-MSI used in this study. Nine characteristic compounds were readily observed for both OLEDs. The observed

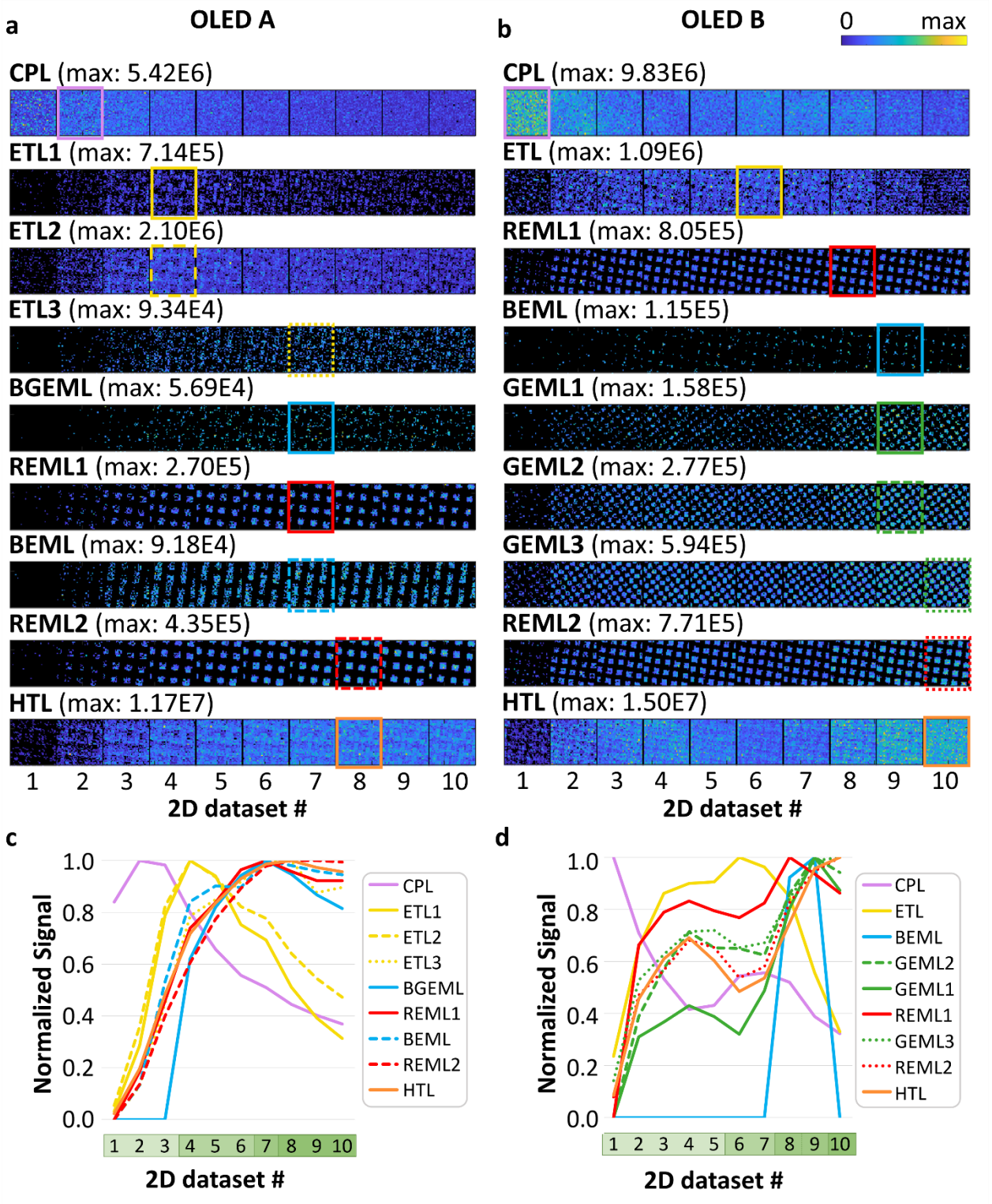

Figure 2. (a, b) Ten consecutive 2D MS images of observed major compounds for OLED A **(a)** and OLED B **(b)**. Scanned area is 410 µm x 410 µm and 400 µm x 400 µm, respectively, with an image pixel size of 10 µm. The ion images are normalized to the maximum signal intensity for each compound across all ten datasets, as denoted in parenthesis. **(c, d)** Normalized average signal intensity for each compound over the ten 2D dataset for OLED A **(c)** and OLED B **(d)**. The boxes in (a) and (b) indicate the 2D data set with the highest average signal presented using the same legends in (c) and (d), respectively.

m/z values matched with the expected mass values within ±10 ppm. A colored box, following the color scheme in **Figure 1b**, is used to denote the 2D dataset that had the maximum average intensity for the compound specified across all ten 2D datasets. Compound identification was supported by matching the expected lateral distribution for each 2D dataset. For example, *m/z* 818.34 representing CPL and *m/z* 678.30 representing HTL are evenly distributed with no special localization as expected for both OLEDs, while compounds representing each emitting layer (REML, BEML, GEML) are matching with localizations of each color pixel (**Tables S1 and S2**). Some compounds are proprietary and their *m/z* values have been removed from the tables, but many of them are known[34-37]. Some apparent partial localization is observed for ETL compounds for both devices, despite these layers having even lateral distribution during device manufacture. ETL is a very thin layer with only tens of nanometer thickness and some underlying emitting layers with pixel specific distributions (e.g., BEML, REML) are present at the same 2D dataset. EML compounds within the ablated laser plume may have affected the ionization efficiencies of ETL compounds, resulting in slightly pixelated patterns in MS images.

Thus obtained 'pseudo depth profiles' of nine compounds can be categorized into roughly four groups. The observed compounds in OLED A have maximum intensities for CPL in the second 2D dataset, ETL1 and ETL2 in the fourth dataset, and ETL3, BGEML, REML1, and BEML in the seventh dataset; then, followed by REML2 and HTL in the eighth dataset. For OLED B, the ordering of 2D datasets for maximum intensity started with the CPL in the first 2D dataset, ETL in the sixth dataset, REML1 in the eight dataset and the BEML, GEML1, and GEML2 in the ninth. Lastly, the GEML3, REML2, and HTL had maximum signal intensities in the tenth 2D dataset. Mass spectra highlighting the CPL, ETL1, REML2, and HTL for the second, fourth, and eighth 2D datasets of OLED A can be seen in **Figure S5** to help visualize the signal differences during the total analysis. For both OLEDs, the sequence of the compounds is consistent with the order of the layering determined during device manufacture, thus demonstrating the resolution of some depth information (**Figure 1b**).

It should be noted that dopant compounds proved to be challenging to observe. This is likely a result of OLEDs having low dopant mol % concentrations, typically under 10% relative to the respective host, with the intent of avoiding quenching processes.[4,5] As the host and dopant are components of a mixed layer, this difference in mol% could lead to ionization suppression of the dopant. The other challenging compound to observe in positive mode is the HIL, which may be more readily ionized in negative mode due to these compounds having high electron affinities.[34,38] Incorporating a matrix may enhance ionization and the number of compounds observed but this would make depth profiling difficult and impractical because the exact position of the MALDI plate might slightly change each time it is ejected for matrix application.

The first few layers are relatively well resolved from other layers in the pseudo depth profiles (e.g., CPL, ETL1/ETL2 in **Figure 2c**); however, deeper layers are very broad and less resolved (e.g., color pixels and HTL in **Figure 2c**). This is likely caused by the difficulty of ablating the inorganic cathode and EIL, that reside between the CPL and the ETL, using the lower laser energies adopted in this study. Scholz *et al.* made a similar argument to justify using higher laser energies for single color OLED LDI-MS depth profiling, where the stack was analyzed at slightly higher laser energy as a compromise to avoid removal of the cathode prior to analysis.[24] The better resolution of depth information for layers near the top of the device was not as apparent in their analysis as they did not use a capping layer in the OLED fabrication process. In our analysis, the observed layers subsequent to the ETL are all comprised of organometallic and organic compounds that absorb the laser energy more efficiently and ablate quicker due to the lack of inorganic layers hindering the absorption of laser energy. The challenge of resolving depth information for lower depths within the OLED structure may also be exacerbated as a result of the lower layers mixing, promoted by repetitive energy influx under and around the repeatedly desorbed/ionized area. Regardless, the analyst obtains partial depth information of the device, highlighted by the reported results.

As presented, the pseudo depth profiles should be carefully interpreted. It is well recognized in the SIMS community that the sputtering rate is not the same for different layers, resulting in incorrect apparent thicknesses of each layer without proper correction of sputtering rate and surface roughening.[39] The sample matrix may also impact the relative ion yields in SIMS analysis, varying for different layers.[40] These considerations should also extend to depth profiling with LDI-MS. Since there is no effort made to calibrate depth scale or ion signals, both x- and y- scale of **Figure 2C** and **2D** may not be linear.

To support the validity of pseudo depth profiles obtained using LDI-MS, DESI-MS was used to perform depth profiling of OLED A. An appropriate choice of DESI solvent can gently dissolve the surface materials during each line scan, producing depth profile when repetitive sampling is performed over the same area. As the lateral resolution is limited for the DESI source employed in the current study, 50 µm or larger, insufficient to image OLED pixels, only depth profiling was explored with multiple line scans for the same area. Six of the nine analytes shown in **Figure 2** were also present in the DESI mass spectra (CPL, ETL2, ETL3, BGEML, REML, and HTL). As shown in **Figure S6**, DESI-MS depth profile has much better resolution with all six compounds having maximum intensities at different line scan number. Most importantly, the order of their appearance is not only matching with the expectations in OLED structure but also consistent with LDI-MS depth profiles, partially supporting the depth profiles obtained by LDI-MS.

OLED Lateral Feature Resolution by LDI-MSI

Chemical information resolved in both lateral and depth dimensions could be useful in developing new devices or solving problems in a failed device. Specifically, it can potentially be used to identify possible contamination sources during the manufacturing process or possible degradation products in malfunctioning devices. Here, lateral distribution assists in verifying each compound due to its expected lateral localization on the device (**Table S1** and **Table S2**). OLED A and OLED B have s-stripe and diamond configuration of the RGB colored pixel components respectively (**Figure 1a**). In OLED A, the red and green pixels are approximately 40 µm x 40 µm in size and the blue pixel is 40 µm x 80 µm. For OLED B, the red pixels are 20 µm x 20 µm, the green are 14 µm x 22 µm, and the blue are 28 µm x 28 µm (**Figure S1**). It should be noted that the pixels are smaller in OLED B than in OLED A, due to image resolu-

tion requirements in handheld cellular devices versus automobile display screens. As mentioned previously, many of the components of the EML are specific to each of the different colored pixels.

For OLED A, the BEML is only expected in the blue pixel and not in the green or red pixel. Likewise, the blue and green pixel host (BGEML) is not expected to be found in the areas containing the red host (REML1). These compounds are selected to serve as indicators for lateral resolution preservation throughout the entire depth profiling experiment, though other observed pixel related compounds could have been candidates for this purpose (**Table S1**). Similarly, in OLED B, the blue host (BEML), green host (GEML1), and red host (REML1) serve as compounds that can be used to indicate the preservation of lateral resolution during depth profiling of OLED B. These compounds should reside in their respective pixels (**Table S2**). No green-only pixel specific compound was observed in OLED A, but three were observed in OLED B. However, as seen in the schematic in **Figure 1b**, the BGEML in OLED A is present in both the green and blue pixel. It should be noted that the fine lateral features of OLED B were more difficult to resolve spatially in the MSI. However, the LDI-MSI images for each compound follows the expected localization (**Figure 3a-c,g-i**) and colocalization plots for the three compounds specified for each OLED suggest that lateral resolution is adequately preserved during the depth profiling. (**Figure 3d-f,j-l**).

LDI-MSI Three-Dimensional Data Visualization

Combination of the depth and laterally resolved chemical information can be used to give a more descriptive spatial distribution of analytes within the OLED. To demonstrate this point, three-dimensional image reconstruction was performed for a few representative compounds shown in **Figure 2a** using MSiReader (v1.02b). Two three-dimensional (3D) image constructions of OLED A were made for color-pixel specific compounds and layer specific compounds. **Figure 4a** shows captures from tracking the color-pixel specific compounds BEML (blue pixel), BGEML (blue/green pixel), and REML1 (red pixel). **Figure 4b** shows captures from tracking layer specific compounds CPL (top layer), REML1 (middle layer), and HTL (bottom layer).

Finding a defect position in three-dimensional space would be useful for OLED research and development when considering failed devices. Though a degradation product at an interface may not be clearly assigned to a corresponding depth position, approximate depth position could still be suggested from the depth profiles. This assignment could be further assisted by lateral distribution of the degradation or contaminant, thus demonstrating the utility of having both depth and lateral chemical composition information. This scenario is demonstrated by monitoring the lithiated adduct of the REML1 ($[Li+REML1]^+$) compound in OLED A (**Figure S7a** and **7b**). The 2D dataset of maximum signal intensity for $[Li+REML1]^+$ is one before that of $REML1^{+\bullet}$ while keeping the same lateral distribution. It is attributed to the laser induced mixing between the layers resulting in the adduct formation of REML1 with lithium ion in the prior layer (ETL).

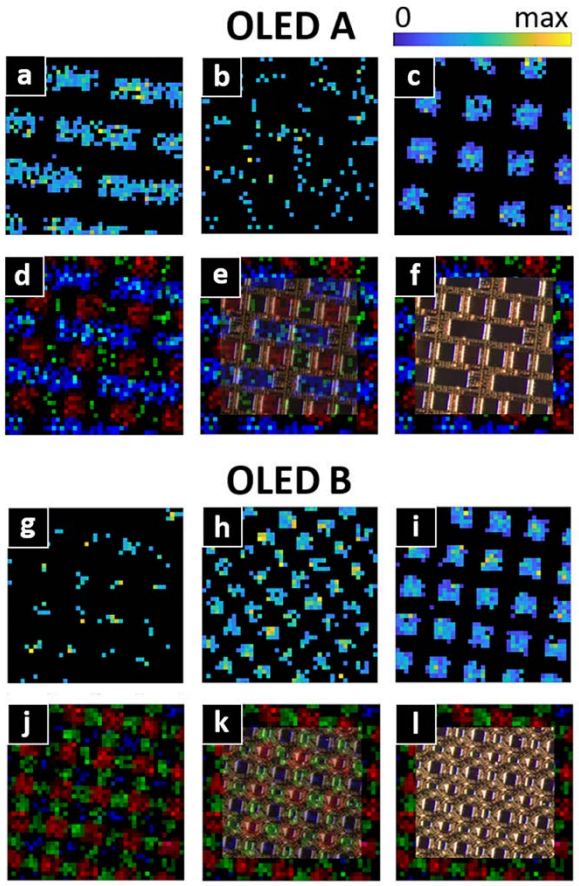

Figure 3. **(a-c)** OLED A LDI-MS images of the 7th 2D dataset for **(a)** BEML, **(b)** BGEML, and **(c)** REML1. **(d-f)** Combination image of **(a-c)** as blue, green, and red, respectively, overlaid with **(d)** 100%, **(e)** 50% or **(f)** 0% transparent optical image. **(g-i)** OLED B LDI-MSI images of the 8th or 9th 2D dataset, dependent on 2D dataset of maximum average intensity, for **(g)** BEML, **(h)** GEML1, and **(i)** REML1. **(j-l)** Combination image of **(g-i)** as blue, green, and red, respectively, overlaid with **(i)** 100%, **(k)** 50% or **(l)** 0% transparent optical image.

Though the $[Li+REML1]^+$ is likely caused by laser induced mixing, this mimics a scenario of two layers interacting and leading to a degradation product. Such a finding in device development would prompt some intervention by the OLED manufacturer. An example of an intervention could be replacing an unstable compound with a more stable analog. Another would be switching out proximate layers that are shown to react with one another over the device lifetime. When device failure occurs, 3D chemical analysis can be performed for malfunctioning areas with this approach to roughly locate any contamination or degradation within the three-dimensional sample space. Once the defect is located, the appropriate adjustment in processing conditions or raw materials can be made.

Through this 3D-LDI-MSI approach, the analyst can be directed to make informed decisions on device improvement but will also need to understand some limitations that arise during the analysis. Most notably, there is thermal diffusion making lower depth layers difficult to resolve. Another artefact that should be considered is laser induced fragmentation during analysis (**Figure S8**). As mentioned, sputtering rate differences for different layers and sample matrix effects should also be

considered. Altogether, the 3D reconstructions may not provide the analyst with exact depth location of a compound within the OLED architecture but will provide information about its location relative to other layers in addition to the lateral distribution of the compound. Given that the analyst will have some prior knowledge about the device (i.e. layering, pixel geometry, compounds) and prior analysis on normal working device, the *a priori* information can serve to help benchmark when looking for contaminants and/or degradation due to aging.

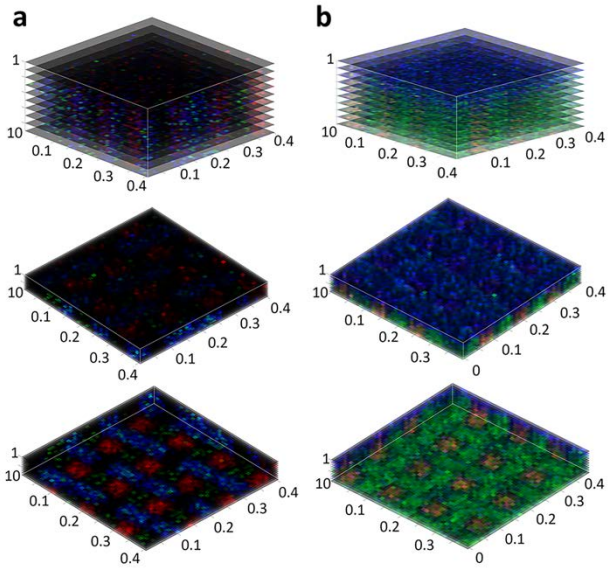

Figure 4. Three-dimensional reconstruction of OLED A LDI-MS images using the same data in **Figure 2a** by stacking MS images of **(a)** color pixel specific compounds, BEML(blue), REML1 (red) , and BGEML (green), or **(b)** layer specific compounds, CPL (blue), REML1 (red), and HTL (green). The z axis is in units of 2D dataset number and the x and y axis are in mm. For both (a) and (b), the top, middle, and bottom images correspond to the views from top-side, top, and bottom, respectively.

CONCLUSIONS

This work demonstrates an application of LDI-MSI to acquire partial depth resolved information while retaining laterally resolved information during OLED analysis. This was realized by using a low laser energy and rastering the laser over the same OLED surface iteratively. The 2D datasets with the maximum average ion intensities for *m/z* values of compounds within the device were shown to follow a logical sequence that is conducive to the layering of the compounds during OLED manufacture. As LDI-MS has been used to guide the assessment of extrinsic and intrinsic degradation processes[17,24,29], we speculate that three-dimensional chemical distribution with LDI-MSI has the potential to do the same. The simplicity of this method, specifically the direct analysis of the OLED without matrix application, is desirable as it limits time requirements on the analyst and the cost of materials needed for sample preparation. Thus, three-dimensional LDI-MSI is a practical method that can provide complimentary information to existing analytical techniques used to assess OLEDs.

LDI-MSI for depth and laterally resolved analysis of OLED screens will complement, not completely replace, existing methods. For example, one downfall of LDI-MSI would be assessing *trans* and *cis* isomers. One such process was suggested by Baranoff *et al.*, showing that sublimation of pure *N,N-transmer* bis-cyclometalated iridium complex, a potential EML compound, during screen fabrication leads to a racemic mixture of the trans and cis isomers. Their assignment was assisted by proton nuclear magnetic resonance and photoluminescence experiments.[41] This may be resolved in LDI-MSI by adopting ion mobility separation (i.e., LDI-ion mobility-MSI).

TOF-SIMS has long been used to analyze organic compounds in semiconductor devices, including OLED, for 2D imaging and 3D profiling. With the recent development in cluster ion source, it can analyze organic compounds up to ~1,000 Da mass range while keeping submicron lateral resolution and nanometer scale depth resolution. LDI-MS approach adopted in this study is inferior to TOF-SIMS in many respects including lateral resolution of a few micron size and depth resolution of ~100nm. Inorganic materials are difficult to sputter or detect with LDI-MS compared to TOF-SIMS. One clear advantage of LDI-MS is medium pressure (75 mTorr in this study compared to ~10^{-9} Torr in TOF-SIMS), allowing the analysis of some partially volatile compounds. 3D imaging in LDI- or MALDI-MS has been typically accomplished by 2D imaging of consecutive tissue sections. Laser ablation with extreme UV and laser ablation electrospray ionization (LAESI) have been previously demonstrated for 3D imaging without sectioning, but the current study is probably the first 3D imaging with a commercial MALDI-MS without multiple sectioning.[42, 43] There are several major concerns in this approach including uncertainties in depth resolution and potential mixing between the layers during LDI sputtering; however, the order of appearance of layer-specific compounds are at least consistent with alternative depth profiling with DESI-MS. It is beyond the scope of this work, but future studies utilizing TOF-SIMS would be necessary to further validate the current approach.

ASSOCIATED CONTENT

Supporting Information

The Supporting Information is available free of charge on the ACS Publications website.

Supplementary figures and tables described in main text (PDF)

AUTHOR INFORMATION

Corresponding Author

* To whom correspondence should be addressed: Tel: 515-294-1235, Email: yjlee@iastate.edu

Author Contributions

The manuscript was written through contributions of all authors. All authors have given approval to the final version of the manuscript.

ACKNOWLEDGMENT

The authors would like to acknowledge funding, samples, and permission to publish provided by Samsung Display Co. Asan, South Korea.

REFERENCES

1. Tang, C.W., VanSlyke, S.A.: Organic electroluminescent diodes. Appl. Phys. Lett. 51, 913–915 (1987).
2. Tang, C.: Organic electroluminescent cell, (1982)
3. Kido, J., Hongawa, K., Okuyama, K., Nagai, K.: White light-emitting organic electroluminescent devices using the poly(N-vinylcarbazole) emitter layer doped with three fluorescent dyes. Appl. Phys. Lett. 64, 815–817 (1994).
4. Tang, C.W., VanSlyke, S.A., Chen, C.H.: Electroluminescence of doped organic thin films. J. Appl. Phys. 65, 3610–3616 (1989).
5. Baldo, M.A., O'Brien, D.F., You, Y., Shoustikov, A., Sibley, S., Thompson, M.E., Forrest, S.R.: Highly efficient phosphorescent emission from organic electroluminescent devices. Nature. 395, 151–154 (1998).
6. Adachi, C., Baldo, M.A., Thompson, M.E., Forrest, S.R.: Nearly 100% internal phosphorescence efficiency in an organic light-emitting device. J. Appl. Phys. 90, 5048–5051 (2001).
7. Nagayama, K., Yahagi, T., Nakada, H., Watanabe, T.T.T., Yoshida, K., Miyaguchi, S.: Micropatterning Method for the Cathode of the Organic Electroluminescent Device. Jpn. J. Appl. Phys. 36, (1997)
8. Koden, M.: OLED displays and lighting. Wiley/IEEE Press, Chichester, United Kingdom (2017)
9. Xia, S.C., Kwong, R.C., Adamovich, V.I., Weaver, M.S., Brown, J.J.: OLED Device Operational Lifetime: Insights and Challenges. In: 2007 IEEE International Reliability Physics Symposium Proceedings. 45th Annual. pp. 253–257. IEEE, Phoenix, AZ, USA (2007)
10. Scholz, S., Kondakov, D., Lüssem, B., Leo, K.: Degradation Mechanisms and Reactions in Organic Light-Emitting Devices. Chem. Rev. 115, 8449–8503 (2015).
11. Schmidbauer, S., Hohenleutner, A., König, B.: Chemical Degradation in Organic Light-Emitting Devices: Mechanisms and Implications for the Design of New Materials. Adv. Mater. 25, 2114–2129 (2013).
12. Schaer, M., Nüesch, F., Berner, D., Leo, W., Zuppiroli, L.: Water Vapor and Oxygen Degradation Mechanisms in Organic Light Emitting Diodes. Adv. Funct. Mater. 11, 116–121 (2001).
13. Fujimoto, H., Suekane, T., Imanishi, K., Yukiwaki, S., Wei, H., Nagayoshi, K., Yahiro, M., Adachi, C.: Influence of vacuum chamber impurities on the lifetime of organic light-emitting diodes. Sci. Rep. 6, 38482 (2016).
14. Penconi, M., Cazzaniga, M., Panzeri, W., Mele, A., Cargnoni, F., Ceresoli, D., Bossi, A.: Unraveling the Degradation Mechanism in FIrpic-Based Blue OLEDs: II. Trap and Detect Molecules at the Interfaces. Chem. Mater. 31, 2277–2285 (2019).
15. Huckaba, A.J., Senes, A., Aghazada, S., Babaei, A., Meskers, S.C.J., Zimmermann, I., Schouwink, P., Gasilova, N., Janssen, R.A.J., Bolink, H.J., Nazeeruddin, M.K.: Bis(arylimidazole) Iridium Picolinate Emitters and Preferential Dipole Orientation in Films. ACS Omega. 3, 2673–2682 (2018).
16. Meerheim, R., Scholz, S., Olthof, S., Schwartz, G., Reineke, S., Walzer, K., Leo, K.: Influence of charge balance and exciton distribution on efficiency and lifetime of phosphorescent organic light-emitting devices. J. Appl. Phys. 104, 014510 (2008).
17. Scholz, S., Meerheim, R., Lüssem, B., Leo, K.: Laser desorption/ionization time-of-flight mass spectrometry: A predictive tool for the lifetime of organic light emitting devices. Appl. Phys. Lett. 94, 043314 (2009).
18. Song, W., So, S.K., Moulder, J., Qiu, Y., Zhu, Y., Cao, L.: Study on the interaction between Ag and tris(8-hydroxyquinoline) aluminum using x-ray photoelectron spectroscopy. Surf. Interface Anal. 32, 70–73 (2001).
19. Lee, S., Kang, J., Ahn, D.A., Shon, H.K., Lee, T.G., Park, S., Suh, M.C., Park, Y.: Sputter Depth-Profile Study of Accelerated Interface Mixing by Thermal Annealing in Solution-Processed Organic Light-Emitting Diodes. Adv. Mater. Interfaces. 1801627 (2018).
20. Nguyen, T.P., Ip, J., Jolinat, P., Destruel, P.: XPS and sputtering study of the Alq3/electrode interfaces in organic light emitting diodes. Appl. Surf. Sci. 172, 75–83 (2001).
21. Jou, J.-H., Lin, Y.-T., Su, Y.-T., Song, W.-C., Kumar, S., Dubey, D.K., Shyue, J.-J., Chang, H.-Y., You, Y.-W., Liang, T.-W.: Plausible degradation mechanisms in organic light-emitting diodes. Org. Electron. 67, 222–231 (2019).
22. Noël, C., Tuccitto, N., Busby, Y., Auer-Berger, M., Licciardello, A., List-Kratochvil, E.J.W., Houssiau, L.: Depth Profiling of Organic Light-Emitting Diodes by ToF-SIMS Coupled with Wavelet–Principal Component Analysis. ACS Appl. Polym. Mater. 1, 1821–1828 (2019).
23. Heil, H., Steiger, J., Karg, S., Gastel, M., Ortner, H., von Seggern, H., Stößel, M.: Mechanisms of injection enhancement in organic light-emitting diodes through an Al/LiF electrode. J. Appl. Phys. 89, 420–424 (2001).
24. Scholz, S., Walzer, K., Leo, K.: Analysis of Complete Organic Semiconductor Devices by Laser Desorption/Ionization Time-of-Flight Mass Spectrometry. Adv. Funct. Mater. 18, 2541–2547 (2008).
25. Chen, S., Xiong, C., Liu, H., Wan, Q., Hou, J., He, Q., Badu-Tawiah, A., Nie, Z.: Mass spectrometry imaging reveals the sub-organ distribution of carbon nanomaterials. Nat. Nanotechnol. 10, 176–182 (2015).
26. Xue, J., Liu, H., Chen, S., Xiong, C., Zhan, L., Sun, J., Nie, Z.: Mass spectrometry imaging of the in situ drug release from nanocarriers. Sci. Adv. 4, eaat9039 (2018).
27. Le Pogam, P., Legouin, B., Geairon, A., Rogniaux, H., Lohézic-Le Dévéhat, F., Obermayer, W., Boustie, J., Le Lamer, A.-C.: Spatial mapping of lichen specialized metabolites using LDI-MSI: chemical ecology issues for Ophioparma ventosa. Sci. Rep. 6, 37807 (2016).
28. Sultana, N., Demarais, N.J., Shevchenko, D., Derrick, P.J.: Laser Desorption/Ionization Mass Spectrometry of Perovskite Solar Cells: Identification of Interface Interactions and Degradation Reactions. Sol. RRL. 2, 1800022 (2018).
29. Tachibana, Y., Nakajima, Y., Isemura, T., Yamamoto, K., Satoh, T., Aoki, J., Toyoda, M.: High Spatial Resolution Laser Desorption/Ionization Mass Spectrometry Imaging of Organic Layers in an Organic Light-Emitting Diode. Mass Spectrom. 5, A0052–A0052 (2017).
30. Jun, J.H., Song, Z., Liu, Z., Nikolau, B.J., Yeung, E.S., Lee, Y.J.: High-Spatial and High-Mass Resolution Imaging of Surface Metabolites of *Arabidopsis thaliana* by Laser Desorption-Ionization Mass Spectrometry Using Colloidal Silver. Anal. Chem. 82, 3255–3265 (2010).
31. Strupat, K., Kovtoun, V., Bui, H., Viner, R., Stafford, G., Horning, S.: MALDI produced ions inspected with a linear ion trap-orbitrap hybrid mass analyzer. J. Am. Soc. Mass Spectrom. 20, 1451–1463 (2009).
32. Korte, A.R., Yandeau-Nelson, M.D., Nikolau, B.J., Lee, Y.J.: Subcellular-level resolution MALDI-MS imaging of maize leaf metabolites by MALDI-linear ion trap-Orbitrap mass spectrometer. Anal. Bioanal. Chem. 407, 2301–2309 (2015).
33. Robichaud, G., Garrard, K.P., Barry, J.A., Muddiman, D.C.: MSiReader: An Open-Source Interface to View and Analyze High Resolving Power MS Imaging Files on Matlab Platform. J. Am. Soc. Mass Spectrom. 24, 718–721 (2013).
34. Yoshida, H., Yoshizaki, K.: Electron affinities of organic materials used for organic light-emitting diodes: A low-energy inverse photoemission study. Org. Electron. **20**, 24-30 (2015).
35. Lee, J., Jeong, C., Batagoda, T., Coburn, C., Thompson, M.E., Forrest, S.R.: Hot excited state management for long-lived blue phosphorescent organic light-emitting diodes. Nature Communications. **8**, 15566 (2017).
36. Sato, T., Miyamae, T., Ohata, H., Tsutsui, T.: Direct observations of the charge behavior of a high-efficiency blue organic light-emitting diode under operating conditions using electric-field-induced doubly resonant sum-frequency-generation vibrational spectroscopy. Org. Electron. **74**, 118-125 (2019).
37. Patil, V.V., Lee, K.H., Lee, J.Y.: Universal blue emitters for high efficiency thermally activated delayed fluorescence and fluorescent organic light-emitting diodes. Dyes and Pigments. **174**, 108070 (2020).

38. Kim, J., Yamamoto, K., Iimura, S., Ueda, S., Hosono, H.: Electron Affinity Control of Amorphous Oxide Semiconductors and Its Applicability to Organic Electronics. Adv. Mater. Interfaces. 5, 1801307 (2018).
39. Taylor, A.J., Graham, D.J., Castner, D.G.: Reconstructing accurate ToF-SIMS depth profiles for organic materials with differential sputter rates. The Analyst. 140, 6005–6014 (2015).
40. Shard, A.G., Havelund, R., Spencer, S.J., Gilmore, I.S., Alexander, M.R., Angerer, T.B., Aoyagi, S., Barnes, J.-P., Benayad, A., Bernasik, A., Ceccone, G., Counsell, J.D.P., Deeks, C., Fletcher, J.S., Graham, D.J., Heuser, C., Lee, T.G., Marie, C., Marzec, M.M., Mishra, G., Rading, D., Renault, O., Scurr, D.J., Shon, H.K., Spampinato, V., Tian, H., Wang, F., Winograd, N., Wu, K., Wucher, A., Zhou, Y., Zhu, Z.: Measuring Compositions in Organic Depth Profiling: Results from a VAMAS Interlaboratory Study. J. Phys. Chem. B. 119, 10784–10797 (2015).
41. Baranoff, E., Suàrez, S., Bugnon, P., Barolo, C., Buscaino, R., Scopelliti, R., Zuppiroli, L., Graetzel, M., Nazeeruddin, Md.K.: Sublimation Not an Innocent Technique: A Case of Bis-Cyclometalated Iridium Emitter for OLED. Inorg. Chem. 47, 6575–6577 (2008).
42. Kuznetsov, I., Filevich, J., Dong, F., Woolston, M., Chao, W., Anderson, E.H., Bernstein, E.R., Crick, D.C., Rocca, J.J., Menoni, C.S.: Three-dimensional nanoscale molecular imaging by extreme ultraviolet laser ablation mass spectrometry. Nat. Commun. 6, 6944 (2015).
43. Nemes, P., Barton, A.A., Vertes, A.: Three-Dimensional Imaging of Metabolites in Tissues under Ambient Conditions by Laser Ablation Electrospray Ionization Mass Spectrometry. Anal. Chem. 81, 6668–6675 (2009).

For Table of Contents Use Only

Three-Dimensional Profiling of OLED by Laser Desorption Ionization-Mass Spectrometry Imaging

Andrew E. Paulson, Young Jin Lee*

OLED structures were analyzed with LDI-MSI to produce both lateral and depth resolved information, allowing the analyst to locate compounds of interest within 3D space.